ADDITIVE MANUFACTURING OF A DEPLOYABLE MONOLITHIC CAMERA COVER FOR PLANETARY EXPLORATION

Maya Roman, Adrian Cheng, and Christine Gebara

Jet Propulsion Laboratory, California Institute of Technology, Pasadena, California, 4800 Oak Grove Dr., Pasadena, CA 91109, USA

ABSTRACT

Camera covers mechanisms are commonly used to protect optical instruments during the launch and landing of various spacecraft used for planetary exploration. These mechanisms have two basic functions: protect optics from foreign objects and debris while stowed and move out of the camera's field of view when deployed. Mechanisms of this sort are easily over engineered, with the final assembly consisting of dozens of piece-parts. This project presents a design that takes advantage of additive manufacturing to combine components, including flexures that deploy the cover. The proposed design would significantly decrease part count and cost while maintaining the function and reliability of traditional camera cover mechanisms. As part of the design development, the performance of printed nylon and Ti-6Al-4V springs were tested and compared to analytical values.

INTRODUCTION

Cameras are key instruments used on nearly every planetary exploration mission, such as the recent Martian Insight lander and the Perseverance rover. Cameras are used for hazard avoidance, navigation, imaging rocks or soil of scientific interest, and to inform operators about spacecraft health. Some missions use imaging during spacecraft Entry, Descent, and Landing (EDL) onto the planet's surface which expose the cameras to extreme debris filled environments. Deployable cover mechanisms protect the cameras and their lenses during EDL and rotate out of the cameras' Fields of View (FOVs) once the spacecraft has landed safely [1]. As a simple, commonly used, spring-driven mechanism, the camera cover was identified as an assembly that could be improved with Additive Manufacturing (AM) using part consolidation and an integrated compliant hinge.

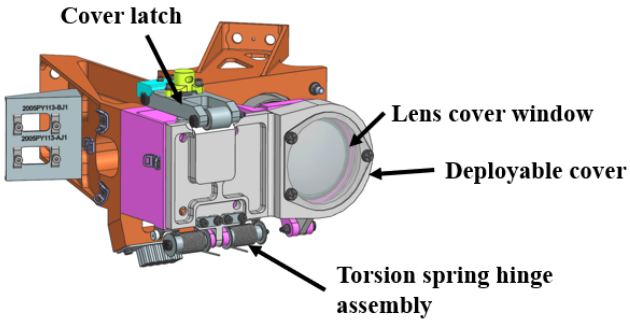

Figure 1: Heritage Mars rover camera cover design.

Many compliant hinge designs exist [2][3][4], but few achieve the rotational stroke required of a camera cover to move outside of a camera's FOV, leading this work to focus on spiral springs as the compliant hinge elements of the camera cover design.

SPIRAL SPRING DESIGN METHODOLOGY

In the application of a camera cover, there are three positions of interest that influence the design of the spring hinge, illustrated in Figure 2. The printed position of the spring, where the spring is fully relaxed, the deployed position, where the spring is loaded to the seating torque, and the stowed position, where the spring is loaded to the actuation torque. The desired stations and torques result in a required stiffness the spring must meet, which can be defined by the geometric dimensions of the spring through spring design equations, described in Equations 1, 2, and 3. Additionally, there are industry standard rules of thumb for designing a spiral spring, $3 < - < 15$, and $1000 < - < 3000$ [5].

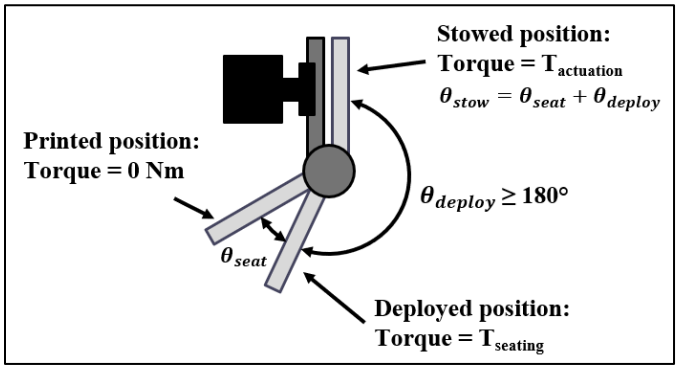

Figure 2: Diagram of camera cover positions of interest for spring design.

$$= \tag{1}$$

$$= \frac{}{6} \tag{2}$$

$$\frac{+}{2} \tag{3}$$

Table 1: Spiral spring equation variables

Symbol	Variable	Symbol	Variable	Symbol	Variable	Symbol	Variable
	Torque	*k*	Torsional stiffness		Number of turns		Inner diameter
b	Width	*t*	Thickness		Angular displacement		Outer diameter
L	Length	*E*	Material elastic modulus				

MULTI-JET FUSION NYLON SPIRAL SPRINGS

Initial printed spiral spring prototypes were Multi-Jet Fusion (MJF) printed PA12 nylon springs. Figures 3a and 3b show the two spring variants that were printed and tested, both with a

targeted stiffness of 0.79 N*mm/degree. The spring parameters are listed in Table 2. The springs feature a hexagonal key in the bottom, and an arm that extends from the outer end of the spring to the center to interface with the torque gauge during testing. To ensure accurate measurements, the nylon springs were designed such that the torque required to twist the spring 200° was half of the maximum torque capability of the torque gauge used to test the spring.

(a) *(b)* *(c)*

Figure 3: MJF nylon spiral springs (a) 17186777-1 & (b) 17186778-1, & (c) the nylon spiral spring test setup.

Table 2: MJF Printed Nylon Spiral Spring Specifications

Parameter	Units	1718777-1	1718778-1
Width, *b*	mm	9.5	9.5
Thickness, *t*	mm	2.2	2.2
Inner diameter,	mm	12.6	9.5
Outer diameter,	mm	93	110
Calculated length, *L*	Mm	2223	2215
Calculated torsional stiffness, *k*	**N*mm/degree**	**0.79**	**0.79**

To test the nylon spiral springs, the center of the spring was fixed with an Allen key, and the outer end of the spring was driven through the torque gauge attached at the center of the spring. The torque gauge was a Waters 651C-3 torque gauge, and the angular displacement was measured manually using a protractor, both shown in Figure 3c. As both measurements were taken manually, multiple measurements were made at discrete points throughout the springs' strokes.

LASER POWDER BED FUSION TI-6AL-4V SPIRAL SPRINGS

The second set of spiral springs tested for this research were Ti-6Al-4V G23 (ELI) springs printed via Laser Powder Bed Fusion (L-PBF). Four springs of three designs were printed on an EOS M290, shown on the print bed in Figure 4. The prints went through a stress relief cycle at a local vendor, and bandsaw operations for removal from the print bed. No other post-processing was performed on the springs, leaving them with the as-printed surface finish.

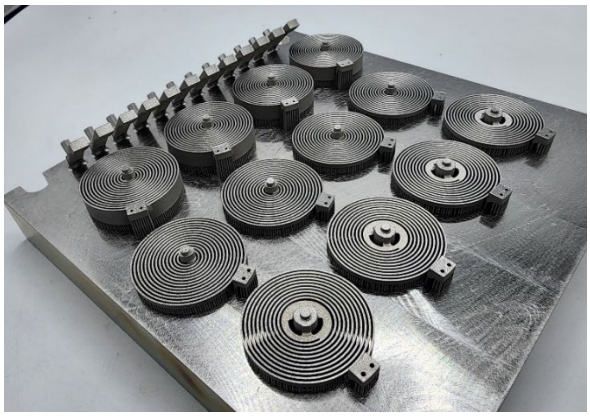

Figure 4: Ti-6Al-4V spiral springs on the print bed.

All spring variations were designed with a deployment angle of 180°, and a seating angle of 20°. The springs shown in Figures 5a and 5b were designed to produce an actuation torque of 0.2 N*m, similar to that of individual springs on heritage Mars rover camera cover assemblies. Spring design 17186798-1 (98) featured a smaller inner diameter, requiring a different number of turns to reach a similar length and stiffness as the 17186797-1 (97). The third spring design, 17186799-1 (99) and shown in Figure 5c had the same specifications as 97, but with a width four times larger, resulting in a projected stiffness and actuation torque four times greater than 97. Each spring was inspected and new estimated spring rates, or torsional stiffnesses, were calculated using the as-printed dimensions of the springs, summarized in Table 3.

(a) *(b)* *(c)*

Figure 5: The three variants of titanium springs: (a) 17186797-1, (b) 17186798-1, & (c) 17186799-1.

Table 3: Ti-6Al-4V Spiral Spring Specifications

Spring P/N		17186797-1					17186798-1					17186799-1				
SN		Target	001	002	003	004	Target	001	002	003	004	Target	001	002	003	004
b	mm	2.45	2.81	2.84	2.78	2.80	2.45	2.74	2.74	2.78	2.69	9.78	10.21	10.17	10.20	10.19
t	mm	0.80	0.80	0.83	0.82	0.82	0.80	0.82	0.83	0.82	0.82	0.80	0.83	0.83	0.83	0.83
	mm	7.78	7.69	7.68	7.68	7.70	20.00	19.78	19.70	19.76	19.72	7.78	7.80	7.74	7.84	7.81
	mm	52.00	51.58	51.56	51.55	53.56	52.00	51.33	51.49	51.84	52.02	52.00	52.16	51.96	52.30	52.16
Calc. *L*	mm	1304	1293	1293	1292	1337	1131	1117	1118	1125	1127	1304	1308	1303	1312	1308
Calc. *k*	**N*mm/degree**	**1.00**	**1.14**	**1.28**	**1.24**	**1.22**	**1.16**	**1.42**	**1.47**	**1.39**	**1.34**	**4.00**	**4.69**	**4.65**	**4.67**	**4.60**

All three spring designs included a hexagonal socket feature, highlighted in Figure 6a, similar to that on the nylon springs for attaching the spring to a test stand. For better printability, the arm that reaches from the outer winding to the center spring axis was printed as a separate part with holes for bolting the arm to the spring body, seen in the top left of the print bed in Figure 4.

However, the titanium springs were evaluated with a new test stand that did not require the center axis arms, and they were not installed or used.

The new test stand used an actuator to drive one side of the Unit Under Test (UUT), in this case a spiral spring. In-line with the actuator and spring was a rotary torque sensor, recording the angular position and the torque as the spring was loaded and unloaded. The center of the spring under test was connected to the sensor and actuator by a hexagonal standoff bolted on a plate that was bolted to the sensor adapter. The outer winding was held in place by a bracket that sat around the side of the tab on the outer diameter, shown in Figure 6b. The test stand drove the center of the spring to the desired angular displacement at a constant, semi-static angular velocity, held the position for 10 seconds, and returned the spring to the unloaded position at the same constant speed, all while the torque sensor recorded the torque and position.

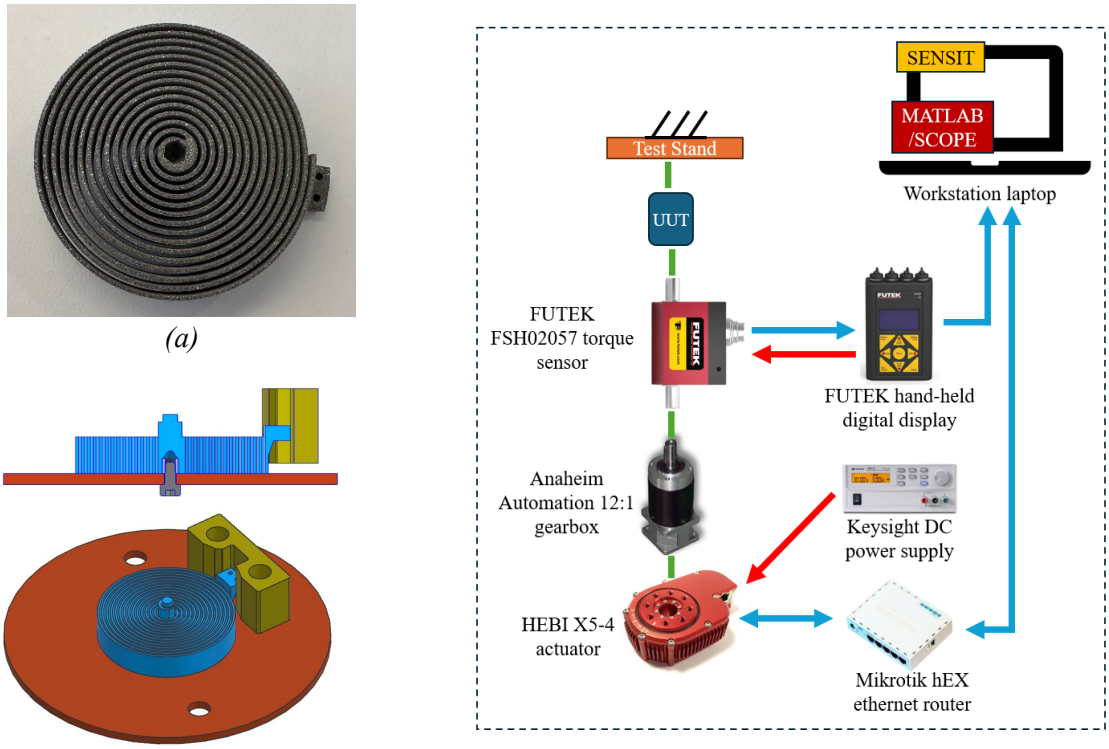

Figure 6: (a) The hexagonal socket feature in the bottom of the Titanium springs, (b) a cross-section and isometric view of the spring interfaces to the test stand, & (c) a system diagram of the torsion test stand.

RESULTS & DISCUSSION

The torque versus angular displacement measurements from the printed nylon springs were fit to linear regression models, plotted alongside the experimental data points in Figure 7. The results from both springs support a linear relationship between the torque and the rotation angle, with an R-squared value for 17186777-1 of 0.998 and an R-squared value of 0.996 for spring 17186778-1. The slopes returned from the models are equivalent to the torsional stiffnesses of the springs, listed in Table 4 and varied by 10-13% from the predicted stiffnesses.

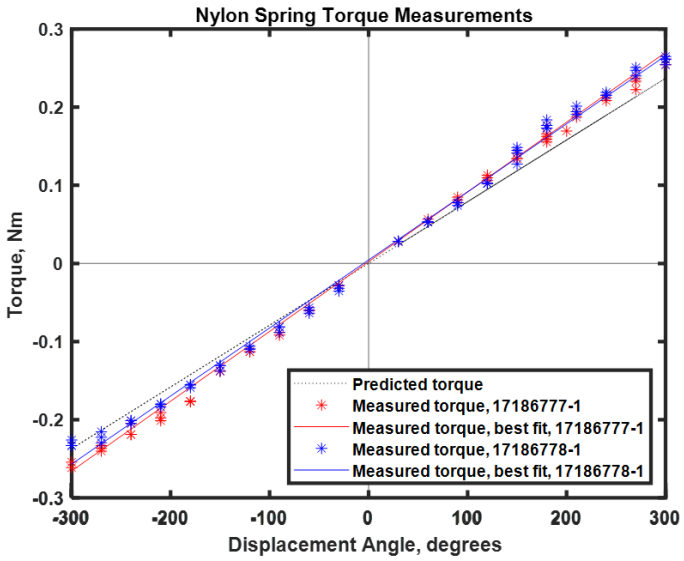

Figure 7: Nylon spiral spring torque versus displacement measurements.

Table 4: Nylon Spiral Spring Torsional Stiffnesses

	Units	1718777-1	1718778-1
Design target torsional stiffness	N*mm/degree	0.790	0.793
Experimental torsional stiffness	N*mm/degree	0.893	0.871
Percent deviation	%	12.9	9.8

The experimental results from the L-PBF printed titanium springs did not correlate well with the analytical predictions. Figures 8a, 8b, and 8c plot the trials for each spring with the predicted torque versus displacement plots, which have very different slopes. The springs were much softer, or had much lower stiffnesses than designed for, however, they still exhibited linear stiffnesses. The data from each trial were fit to linear regression models, which also supported a linear relationship between the angular displacement and the torque, with the coefficient of determination (i.e., R-Squared) values for each trial ranging between 0.891 to 0.997. The torsional stiffnesses from the linear regression models had errors ranging between 81% to 91% compared to the expected stiffnesses, listed in Table 5.

Looking at the experimental stiffnesses in more detail, it was observed that the cases in which the spring was loaded by twisting in on itself (i.e., winding up) consistently had higher stiffnesses than the cases which loaded the springs by opening them up (i.e., unwinding). The plot shown in Figure 8c labels the stiffnesses for spring design 99, with the data points indicating spring loading into itself above the data points for loading by opening of the spring. This behavior would be expected, as the spring windings come in contact with each other as the springs are wound tighter around the inner diameter, and the additional friction from the rough, as-printed surface finish would increase the torque required to drive the spring tighter. Two-tailed t-tests confirmed that for each spring set, there is a statistically significant difference between the stiffnesses depending on the direction of spring loading. The p-value, or the probability that the mean

difference between directional stiffnesses was zero, was less than or equal to 0.002, or 0.2%, for each spring set.

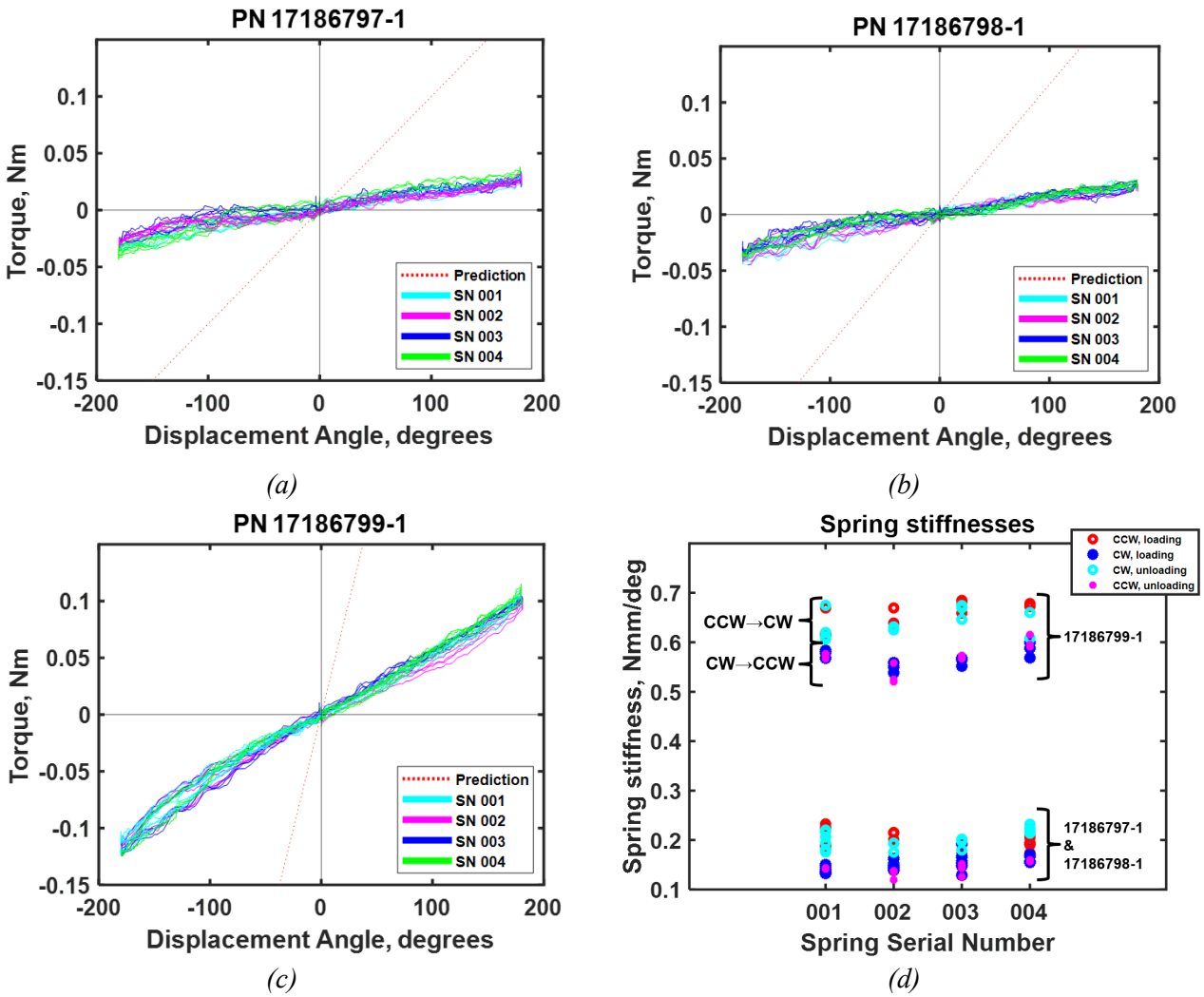

Figure 8: Torque vs angular displacement plots for (a) 17186797-1, (b) 17186798-1, (c) 17186799-1, & (d) plot of the experimental stiffnesses for all titanium springs.

Table 5: Ti-6Al-4V Spiral Spring Torsional Stiffnesses

	Units	1718797-1	1718798-1	1718799-1
Design target	N*mm/degree	1.00	1.16	4.00
Average experimental, CCW→CW	N*mm/degree	0.173	0.203	0.647
Average experimental, CW→CCW	N*mm/degree	0.146	0.152	0.569
Average experimental, overall	N*mm/degree	0.160	0.179	0.606

One theory for the lower-than-expected torsional stiffnesses was that the springs may have had high porosity due to their thin cross-sections and since they did not undergo Hot Isostatic Pressing (HIP) treatment. High porosity would affect their second moments of area, and therefore change the expected spring performance. To investigate this theory, springs of each design were cut across their center axes, polished, and imaged to assess their porosity. Based on visual

inspection of the images, some of which are shown in Figure 9, the spring windings appear to have low porosity, meaning it is unlikely that the porosity is a major contributor to the low spring stiffnesses. Note that the surfaces at the top of the sections in Figures 9b and 9c are the faces of the springs that had support material that was coarsely cut off, resulting in the rougher surface finish. An additional interesting observation from these photos is the slight curved nature of the windings' cross-sections, which could have contributed to lower-than-expected stiffness witnessed during testing.

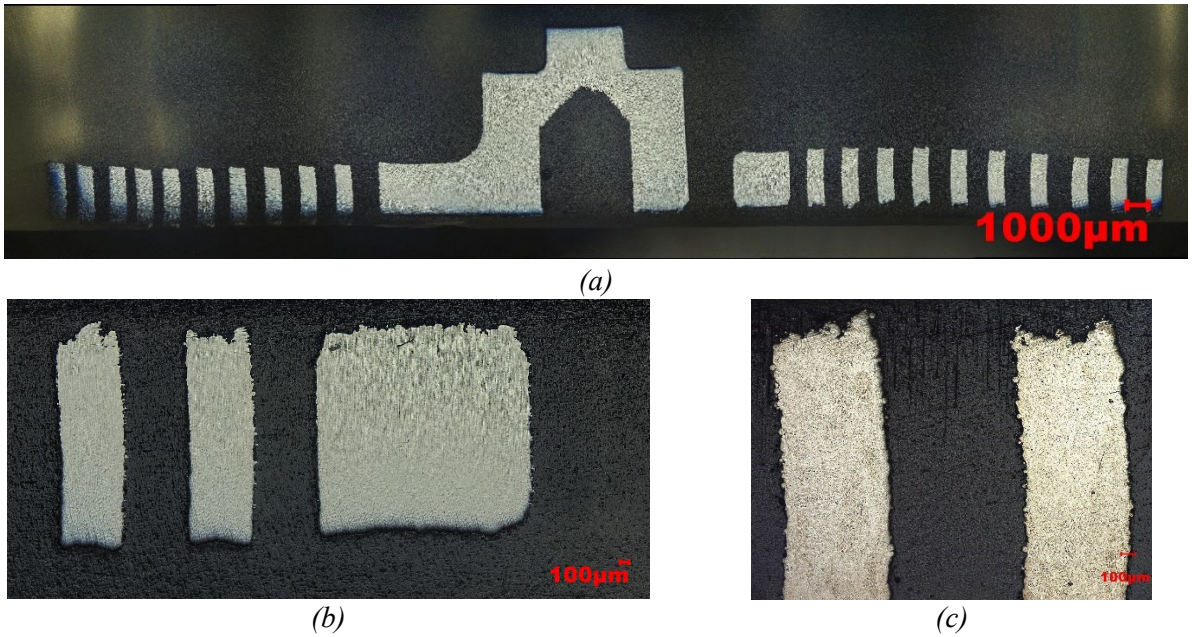

(a) *(b)* *(c)*

Figure 9: Microscopic photos of the cross-section of spiral spring 1718799-1, serial number 002.

There are a few other possible explanations for the discrepancies between the expected and tested stiffness values. The spring parameters were calculated, in part, based on industry recommended ratios between the length, width, and height of the spring. These ratios are likely based on empirical data for traditionally manufactured spiral springs which are generally made at a smaller scale than these printed springs. Since the sizes of the printed springs were beyond traditional spiral spring parameters, the industry "rules of thumb" may not apply, resulting in unrealistic predictions. The thin-walled nature of the springs, only 0.8 mm thick, in addition to the curvature, also likely affected the as-printed material properties, potentially invalidating the expected values which rely on assumed properties based on the printing process and stress relief standards. Additionally, twisting of the springs in and out of the plane of the spiral was observed in most test cases, shown in Figure 10, which could also affect the stiffness about the spiral's center axis.

Figure 10: Springs under test experiencing cross-section twist.

While the stiffnesses varied greatly from the expected values, the values for springs of all three designs consistently deviated from the design target stiffnesses by an average factor of 0.13. That value could be used as a knockdown factor and evaluated in further additively manufactured spring designs. As the next step in implementing the springs into a more monolithic camera mechanism, the spring designs were modified to include the experimental knockdown factor of 0.13 and implemented as the hinges in a camera cover body. The body, including the fixed base that attaches to the spacecraft, the spiral spring hinges, and the deployable cover, was integrated with a heritage Hold-Down Release Mechanism (HDRM) to hold the cover closed. The heritage camera cover mechanism and the new mechanism are showed side by side in Figure 11. This proposed mechanism has a part count less than half of the heritage design, the majority of which are from the HDRM assembly, and a decreased mass, as listed in Table 6.

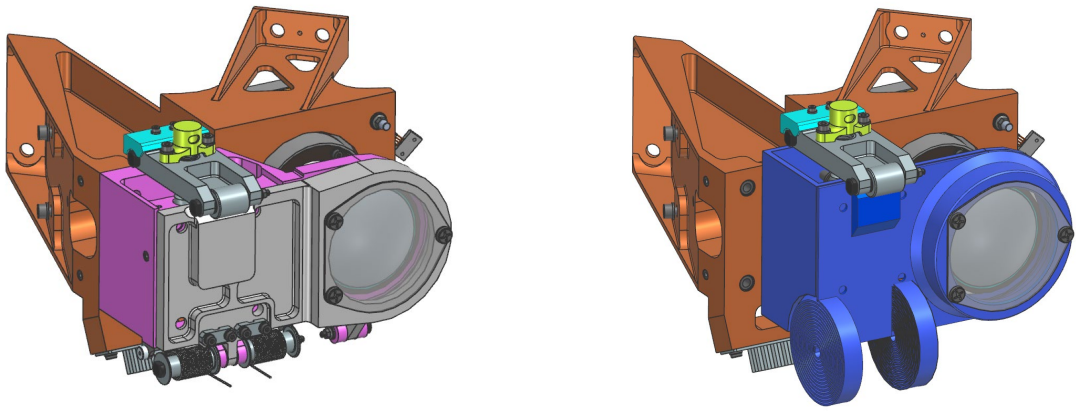

(a) *(b)*

Figure 11: a) The heritage camera cover & b) The proposed camera cover with integrated spiral springs.

Table 6: Comparison of heritage versus proposed camera cover mechanisms.

	Heritage M2020 camera cover	Proposed monolithic mechanism
Part count	137	52
Mass	~0.66 kg	~0.45 kg

SUMMARY & FUTURE WORK

In an effort to consolidate parts in a deployable mechanism using additive manufacturing, spiral springs were designed, printed, and tested in both nylon and Ti-6Al-4V. The multi-jet fusion printed nylon springs behaved as designed based on spiral spring design equations, but the laser powder-bed fusion printed titanium springs exhibited lower stiffnesses than predicted. An iterated version of the titanium spring was integrated into a monolithic housing for an additively manufactured deployable camera cover design.

Future work should further investigate the cause behind the discrepancy between the expected and experimental stiffnesses of the titanium springs. Printing and mechanically testing coupons with the same thickness, curvature, and print orientation as the spring windings would yield the thin-walled material properties and could be used to revise the expected spring

characteristics. A test fixture that can better accommodate the radial displacement of the outer winding while the spring is loaded and unloaded may help reduce twisting of the spring. A low-friction baseplate may also prevent out of plane motion completely. The upgraded test fixture could then be used to test a range of springs with different specifications to investigate the validity of the experimental knockdown factor. An updated torsional test fixture could also apply known axial and radial misalignments between the inner and outer diameters of the spring to test the spring's sensitivity to misalignments. The monolithic camera cover housing design should also be further matured before it is then printed and tested, and possibly infused into a space flight mission.

ACKNOWLEDGEMENTS

The research was carried out at the Jet Propulsion Laboratory, California Institute of Technology, under a contract with the National Aeronautics and Space Administration (80NM0018D0004). We want to acknowledge the Research and Technology Development Office for their continued support on this task, Adrian Cheng and the JPL Additive Manufacturing Center for the great work printing and processing the springs, Doug Hoffman for lab space for the torsion test stand, and Greg Agnes for the idea to look at a camera cover mechanism.

REFERENCES

[1] Justin Maki, "The Mars 2020 Engineering Cameras and Microphone on the Perseverance Rover: A Next-Generation Imaging System for Mars Exploration", https://doi.org/10.48577/jpl.JQOSAY, Space Science Reviews, JPL Open Repository

[2] Thalmann, E., and Henein, "Triple Crossed Flexure Pivot Based on a Zero Parasitic Center Shift Kinematic Design", ASME, *J. Mechanisms Robotics*, 2022; 14(4): 045001. https://doi.org/10.1115/1.4053471

[3] Peter Spanoudakis, Lionel Kiener, Florent Cosandier, Daniel Grivon, Philippe Schwab, Nabil Bencheik, "Large Angle Flexure Pivot Development for Future Science Payloads", ESMATS, 2021.

[4] Sicong Wan and Q. Xu, "Design of a new rotational micropositioning mechanism driven by limited-angle torque motor," 10th IEEE International Conference on Nano/Micro Engineered and Molecular Systems, Xi'an, China, 2015, pp. 209-213, https://doi.org/10.1109/NEMS.2015.7147412

[5] Associated Spring, "Engineering Guide to Spring Design", 2021, https://www.asbg.com/engineering-guide-to-spring-design.aspx.